RSC Advances

PAPER

View Article Online
View Journal | View Issue

Cite this: *RSC Adv.*, 2022, **12**, 28128

A bipolar host material for the construction of triplet-energy level for white phosphorescent organic light emitting diodes

Hsin-Yi Wen * and Shou-Yi Ho

Received 16th August 2022
Accepted 17th September 2022

DOI: 10.1039/d2ra05124a

rsc.li/rsc-advances

Efficient white lighting sources based on phosphorescent organic light emitting diodes (PhOLEDs) have been predicted as the next generation of highly efficient general illumination systems. This study proposed a novel host material, CzppT, featuring the characteristics of bipolarity while possessing electron-withdrawing pyridine and electron-donating carbazole groups in the hexaphenylbenzene core, suitable for use in both blue and white PhOLEDs. The CzppT possesses a high triplet energy level and thermally activated delayed fluorescence stable which is confirmed by the high value of T_d (480 °C). The effect of the emission layer deposition method on the characteristics of the device was studied in the dicarbazole derivative fabricated in a hole and electron-only device to ensure the bipolarity of CzppT. A blue PhOLED device exhibited a maximum external quantum efficiency of 11.0% with CIE coordinates (*x*, *y*) of (0.18, 0.41). Moreover, a white PhOLED device doped with a dye has a maximum external quantum efficiency of 11.3%, and CIE coordinates (*x*, *y*) of (0.32, 0.36). These results demonstrate that the hexaphenylbenzene derivative was conveniently synthesized with bipolarity and hole- and electron-transporting ability and high triplet energy level. Moreover, as a host material, it is expected to be applied to bipolar, high EL efficiency OLEDs in the future.

Introduction

Low-energy-consumption lighting has prompted considerable research effort toward its potential use in other high-efficiency products, such as the development of white organic light emitting diodes (WOLEDs) for applications.[1] Based on the techniques of vacuum thermal evaporation, spin-coating used in thin film deposition, and 3D-printing active optoelectronic devices, organic light-emitting diodes (OLEDs) can be fabricated as devices that are light-weight, inexpensive, flexible, and transparent.[2–6] Although OLEDs for lighting applications can be fabricated with low consumption of electrical energy and economical processing, device efficiency and lifetime still remain among the challenges.[7–9]

Efficient white lighting sources based on phosphorescent organic light emitting diodes (PhOLEDs) have been predicted as the next generation of highly efficient general illumination systems. The light emission through radiative relaxation from the spin-statistics can be either a singlet or triplet emitter associated with excitons into the light emitting layer to generate 25% of the singlet and 75% of the triplet with electroluminescent materials for OLEDs.[7,10–12] The PhOLEDs have the advantage that both singlet and triplet states provide 25 and 75% of the excitons, respectively, that radiate in phosphorescent materials to generate highly efficient internal quantum efficiencies (IQEs) of up to 100%; in contrast, with fluorescent materials, only the singlet excitons can decay radiatively, considerably limiting the maximum IQE to just 25%. A higher energy photon caused by the intersystem crossing (ISC) happens when two triplets annihilate to leave the emitter in its higher energy singlet state. White PhOLEDs have been fabricated using two approaches: (i) the stacking of two or more individual layers emitting different colors from among the three primary colors (*i.e.*, essential red, green, and blue emitters) or two emitters of complementary colors (*e.g.*, mixing sky-blue with deep-red) and (ii) the mixing of multiple emitters in a single layer to decrease structural heterogeneity and promote charge injection and transport to the emitting layer (*e.g.*, doping different emitters in the same host component). Problems have arisen when the host material of the emitting layer used for white or blue electroluminescence undergoes the non-radiative processes of reverse intersystem crossing from the triplet excited state (T_1) to the singlet excited state (S_1) and triplet–triplet (T_1–T_1) annihilation to generate the singlet exciton, which decreases device efficiency and electroluminescence.[13] Accordingly, improvements in molecular design have been targeted to ensure a high energy gap and a triplet excited state to avoid T_1–S_1 reversing and T_1–T_1 annihilation. In 2011, for example, hosts possessing highly twisted configurations and, therefore, high triplet energy levels were employed to prepare highly efficient blue PhOLEDs having appropriate highest occupied molecular orbital (HOMO) energy levels, resulting in improved hole-

Department of Chemical and Materials Engineering, National Kaohsiung University of Science and Technology, Kaohsiung 80778, Taiwan. E-mail: hsinyiwen@nkust.edu.tw

injection properties.[14,15] The problem of T_1–S_1 intersystem crossing can be minimized by ensuring that the triplet energy level of the host material is higher than that of the hole transporting layer (HTL), the electron transporting layer (ETL), and the guest material in the emitting layer. To obtain PhOLEDs exhibiting improved stability and efficiency, we must develop new materials possessing high triplet energy levels. Moreover, we must design molecules that facilitate charge injection and transport from the HTL and ETL to the light emitting film and, thereby, improve device performance significantly. An alternative approach toward high-performance white PhOLEDs is through doping of one or more molecular emitters in a large-energy-gap host having transporting capability; in some reports,[16] this host also functions as an emitting component.

A possible role of a host material having a wide energy gap is related to control over the triplet excited energy level that can confine the triplet excited energy level of the metal complex. An interesting example is that of the hexaphenylbenzene derivatives reported in 2007,[17] where the low degree of π-conjugation, a result of the twisted structure of the bulky hexaphenylbenzene unit, led to wide HOMO–lowest unoccupied molecular orbital (LUMO) energy gaps and steric hindrance, suitable for OLEDs based on a blue phosphorescent complex. Recently, hexaphenylbenzene derivatives bearing non-planar phenyl groups and having high values of T_1 and high glass transition temperatures (T_g) have been reported[18] to possess thermal stabilities greater than those of characteristic materials and, thereby, improved device stability.[19] In addition, several carbazole derivatives have been reported to exhibit high efficiency as hole transporters because their carbazole moieties enhance the hole transporting ability and improve the electroluminescence (EL) properties.[14,19,20] These carbazole derivatives have small singlet–triplet exchange energies (ΔE_{ST})—that is, a small difference in energy between the singlet excited energy and the triplet excited energy—making them among the most attractive candidates for decreasing the driving voltages of OLEDs while ensuring high chemical compatibility with dopants to suppress the dopant aggregation.[21] Pyridine moieties promote electron injection into and electron transport within pyridine-containing ETLs.[22]

Accordingly, in this study we introduced electron-withdrawing pyridine groups[23,24] and electron-donating carbazole groups[25] into a hexaphenylbenzene core to synthesize a bipolar host material—4,4″-dicarbazolyl-2′,3′-dipyridinyl-5′,6′-diphenyl-*p*-terphenyl (CzppT)—for use in PhOLEDs. We obtained this hexaphenylbenzene derivative conveniently from 4,4″-dibromo-2′,3′-dipyridinyl-5′,6′-diphenyl-*p*-terphenyl and dicarbazole in the presence of CuI, crown-6, and K_2CO_3 in DMPU.[26] Herein, we report the EL performance of blue and white PhOLEDs using CzppT as a host material that has a high triplet energy level containing suitably chosen hole- and electron-transporting moieties.

Experimental

Materials

All solvents were distilled from appropriate drying agents prior to use. Commercially available reagents were used without further purification. All reactions were monitored using thin layer chromatography (TLC). Flash column chromatography was performed using SCI silica gel (230–400 mesh, pH 7.0). The synthetic routes are presented in Scheme 1. A well-mixed solution of (*p*-bromophenyl)acetic acid (**1**) and magnesium oxide in N_2 was heated at 340 °C, providing 1,3-bis(*p*-bromophenyl)-2-propanone (**2**), which was collected through distillation, according to a literature procedure.[27] Aldol condensation of **2** and 2,2′-pyridil with KOH in EtOH at 80 °C for 15 min gave 2,5-bis(*p*-bromophenyl)-3,4-di(pyridin-2-yl)cyclopenta-2,4-dienone (**3**). 4,4″-Dibromo-2′,3′-dipyridyl-5′,6′-diphenyl-*p*-terphenyl (**4**) was prepared by the Diels–Alder reaction of (**3**) with diphenylacetylene. The target compound CzppT (**5**) was synthesized *via* the copper(I) iodide aromatic C–N coupling by an Ullmann reaction of carbazole and (**4**) in the presence of copper(I) iodide and 18-crown-6 in DMPU.

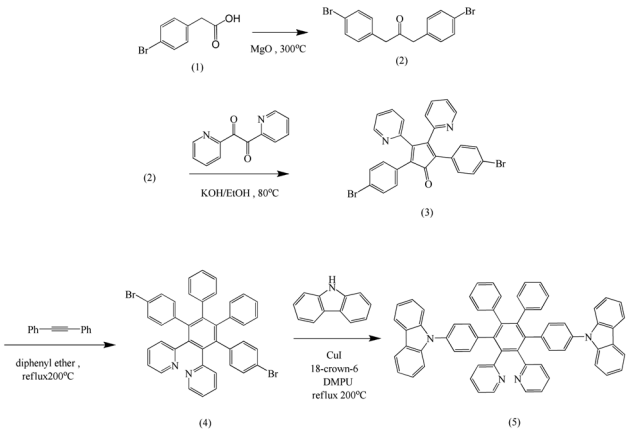

Scheme 1 Synthesis process of CzppT.

1,3-Bis(*p*-bromophenyl)-2-propanone (2)

A well-mixed solution of *p*-bromophenylacetic acid (**1**) (323 g, 1.50 mol) and 94% magnesium oxide (66.5 g, 1.65 mol) was heated at 250 °C under reduced pressure to remove water of condensation. Distillation (340 °C, 1–3 torr) provided a crude product (225 g, 81.6%); recrystallization (EtOH) yielded **2** as colorless platelets (192 g, 60%). ^{1}H NMR (500 MHz, 25 °C, $CDCl_3$; δ, ppm): 7.45 (d, $J = 8.5$ Hz, 4H), 7.01 (d, $J = 8.5$ Hz, 4H), 3.68 (s, 4H).

2,5-Bis(*p*-bromophenyl)-3,4-di(pyrid-2-yl)cyclopenta-2,4-dienone (3)

A mixture of **2** (1.20 g, 3.26 mmol), 2,2′-pyridil (0.52, 2.4 mmol), and EtOH (30 mL) was heated at 78° and the solution of KOH (0.1 g, 1.78 mmol) in EtOH (10 mL) was added dropwise. An exothermic reaction was followed by precipitation of a white solid, which was filtered off, washed thoroughly several times with EtOH, and dried *in vacuo*. This solid was dissolved in boiling ethylene glycol and stirred for 15 min. After cooling to room temperature over 3 h, the dark red crystals were filtered off, washed with MeOH, and dried *in vacuo* (0.995 g, 74%). ^{1}H NMR (300 MHz, 25 °C, $CDCl_3$; δ, ppm): 8.35 (d, $J = 4.5$ Hz, 2H),

7.55 (t, J = 9.0 Hz, 2H), 7.38 (d, J = 8.7 Hz, 4H), 7.20 (d, J = 8.1 Hz, 2H), 7.10–7.13 (m, 6H). ESI-MS: m/z 545 (100%, $[M + 1]^+$).

4,4″-Dibromo-2′,3′-dipyridyl-5′,6′-diphenyl-*p*-terphenyl (4)

A mixture of **3** (2.5 g, 4.6 mmol), diphenylacetylene (3.00 g, 16.0 mmol), and phenyl ether was heated at 200 °C for 24 h, during which time the dark purple color vanished. After cooling, the precipitate was filtered off and recrystallized (DMSO) to yield a white powder (2.58 g, 80%). ^{1}H NMR (300 MHz, 25 °C, $CDCl_3$; δ, ppm): 8.15 (d, J = 4.8 Hz, 2H), 7.20 (t, J = XX Hz, 2H), 6.91 (d, J = 8.7 Hz, 4H), 6.72–6.93 (m, 18H). MALDI-MS: m/z 694.979 (100%, $[M + 1]^+$).

4,4″-Dicarbazolyl-2′,3′-dipyridyl-5′,6′-diphenyl-*p*-terphenyl (5)

A mixture of **4** (1.00 g, 1.10 mmol), carbazole (1.5 g, 8.90 mmol), CuI (0.0272 g, 0.140 mmol), crown-6 (0.124 g, 0.470 mmol), and K_2CO_3 (0.826 g, 5.90 mmol) in 1,3-dimethyl-3,4,5,6-tetrahydro-2(1*H*)-pyrimidinone (DMPU, 3 mL) was heated at 200 °C for 48 h under N_2. After cooling to room temperature, the mixture was quenched with 1 N HCl and then precipitated and partitioned between NH_3 liquor and CH_2Cl_2. The organic phase was concentrated and the residue was then purified chromatographically (Al_2O_3; CH_2Cl_2); recrystallization (Et_2O/CH_2Cl_2) yielded a white solid (0.70 g, 56%). ^{1}H NMR (500 MHz, 25 °C, $CDCl_3$; δ, ppm): 8.29 (d, J = 4.5 Hz, 2H), 8.07 (d, J = 8 Hz, 4H), 7.36 (t, J = 7.5 Hz, 6H), 7.24 (t, J = 7.5 Hz, 4H), 6.89–7.15 (m, 26H). MALDI-MS: calcd for $C_{64}H_{42}N_4$, m/z 866.34; found, m/z 867.0 (100%, $[M + 1]^+$). Elemental analysis: calcd for $C_{64}H_{42}N_4$: C, 88.66; H, 4.88; N, 6.46. Found: C, 88.80; H, 4.69; N, 6.36.

Fabrication and characterization of PhOLEDs

The structures of the devices consist with material as following: 1,3-bis(9*H*-carbazol-9-yl)benzene (mCP), bis(4,6-difluorophenylpyridine) (picolinate) iridium(III) (FIrpic), 2,9-dimethyl-4,7-diphenyl-1,10-phenanthroline (Bcp), 1,3,5-tri[(3-pyridyl)phen-3-yl]benzene (TmPyPB), 1,3,5-tris(*N*-phenylbenzimidazol-2-yl)benzene (TPBi), 4,4′,4″-tris(*N*-carbazolyl) triphenylamine (TCTA), *N*,*N*′-di(1-naphthyl)-*N*,*N*′-diphenylbenzidine (NPB), and bis(1-phenylisoquinoline)(acetylacetonate) iridium(III) [Ir(piq)$_2$acac]. The organic chemicals used in the fabrication of devices were generally purified through high-vacuum, gradient-temperature sublimation. CzppT was purified through flash column chromatography prior to use. Devices were fabricated on glass substrates layered with 170 nm-thick indium tin oxide (ITO) having a sheet resistance of approximately 10 Ω $\square^{-1}$. The substrates were cleaned through ultrasonication in ^{i}PrOH and deionized H_2O, followed by treatment with O_2 plasma. ITO and LiF/Al were employed as the anode and cathode, respectively. All devices were fabricated through vacuum deposition of the materials at 10^{-6} torr. The rates of evaporation and the thicknesses of the organic and metal layers were monitored using quartz oscillators; the deposition rate of the organic compounds was 1.0–1.5 Å s^{-1}. The cathode, comprising LiF/Al, was deposited through sequential evaporation of LiF (deposition rate: 0.1 A s^{-1}) and Al metal (gradient rates: 0.1–5.0 Å s^{-1}) without breaking the vacuum. Considering matching HOMO/LUMO energy levels of the materials, hole-only, electron-only, blue PhOLED, and white PhOLED devices were fabricated to analyze and compare the bipolar properties of Czppt. Devices **a** to **d** were prepared to investigate the mobility and electroluminescence properties. The hole transporting materials were NPB and CzppT; the electron transporting materials were TmPyPB, TPBi, and CzppT. TCTA was used to improve hole transport by facilitating hole injection. To determine the charge-carrier transport and energy transfer to a deep-blue-emitting phosphorescent dopant of CzppT in the thin films, single-charge (hole- and electron-only) devices based on this material were fabricated: a hole-only device having the structure ITO/NPB (30 nm)/TCTA (5 nm)/CzppT (50 nm)/NPB (20 nm)/LiF (0.8 nm)/Al (200 nm) and an electron-only device having the structure ITO/Bcp (30 nm)/CzppT (50 nm)/TPBi (20 nm)/LiF (0.8 nm)/Al (200 nm). CzppT was tested as the host material for blue and white PhOLEDs; the device structures were ITO/NPB (45 nm)/TCTA (5 nm)/CzppT:FIrpic (30 nm)/TmPyPB (45 nm)/LiF (0.8 nm)/Al (200 nm) and ITO/NPB (45 nm)/TCTA (5 nm)/CzppT:FIrpic:Ir(piq)$_2$acac (30 nm)/TmPyPB (45 nm)/LiF (0.8 nm)/Al (200 nm), respectively. The doping concentration of FIrpic was 20% in devices **c** and **d**; 0.14% of Ir(piq)$_2$acac was added in device **d**. The luminance–current density–voltage characteristics were recorded simultaneously with the EL spectra by combining the spectrometer with a Keithley 2400 programmable voltage–current source after the devices had been sealed in a N_2-filled glove box. All measurements were made at room temperature under ambient conditions. The active area of each device was 3 mm^2.

Measurements

^{1}H NMR spectra were recorded using Varian UNITY INOVA-500 and Varian VXR-300 MHz NMR spectrometers. Matrix-assisted laser desorption/ionization time-of-flight mass spectrometry (MALDI-TOF MS) was performed using Bruker Autoflex III TOF/TOF and Bruker APEX II (MASS) mass spectrometers. Elemental analyses were performed using an Elementar vario EL III Heraeus CHNOS Rapid F002 elemental analyzer. The ionization potentials and HOMO energy levels were measured using ultraviolet photoelectron spectroscopy (Thermo VG-Scientific, Sigma Probe). Photoluminescence (PL) and absorption spectra were measured using a Hitachi F-4500 fluorescence spectrophotometer and a PerkinElmer Lambda35 UV-Vis spectrometer, respectively. To measure the triplet energy of CzppT, the phosphorescence spectrum of CzppT was obtained at 77 K using a Hitachi F-4500 phosphorescence spectrophotometer. Thermogravimetric analysis (TGA) was performed using a PerkinElmer thermogravimeter (model PYRIS 1 TGA) under a dry N_2 gas flow at a heating rate of 10 °C min^{-1}. Colorless crystals of CzppT suitable for X-ray diffraction studies were grown through vapor diffusion ($CHCl_2/Et_2O$, 1 : 1) at room temperature. Single-crystal X-ray diffraction (XRD) data were obtained using a Bruker APEX DUO charge-coupled device (CCD) diffractometer. The measurements were performed at 100 K using graphite-monochromated Mo-Kα radiation (λ = 0.71073 Å). The thicknesses of the layers were measured using a Dektak 150 surface profiler. The EL spectra and CIE coordinates of the

devices were measured using a PR650 spectrometer. Additionally, the triplet energy level of host materials is very important, because in deep blue PHOLEDs high triplet energy charge transport materials, host and dopant materials must be newly synthesized. Common charge transport materials for red and green or sky blue PHOLEDs could not be used in deep blue PHOLEDs because of triplet exciton quenching by charge transport materials originating from the low triplet energy of charge transport materials. Phosphorescence spectra were recorded at 77 K in 10^{-4} M $CHCl_3$ solution of CzppT. All measurements were made at room temperature (except triplet energy level) under ambient conditions. The active area of the device was 3 mm^2.

Results and discussion

Synthesis and characterization

Scheme 1 displays the molecular structure of CzppT and its synthetic route. 1,3-Bis(*p*-bromophenyl)-2-propanone (**2**) was isolated in 60% yield from the reaction of 2-(*p*-bromophenyl) acetic acid in the presence of magnesium oxide under N_2 at 300 °C. Aldol condensation of **2** and 2,2′-pyridil in the presence of KOH in EtOH at 80 °C for 15 min gave 2,5-bis(*p*-bromophenyl)-3,4-di(pyrid-2-yl)cyclopenta-2,4-dienone (**3**) in a yield of 74%. We obtained 4,4″-dibromo-2′,3′-dipyridyl-5′,6′-diphenyl-*p*-terphenyl (**4**) in 80% yield after the Diels–Alder reaction of **3** with diphenylacetylene. Finally, the target compound CzppT (**5**) was obtained in 56% yield after aromatic C–N coupling (Ullmann reaction) of **4** and carbazole in the presence of copper(I) iodide and crown-6 in DMPU.[26]

We purified CzppT chromatographically through Al_2O_3, followed by sublimation to produce a very pure powder. ^{1}H NMR spectroscopy, mass spectrometry, and elemental analysis confirmed the chemical structures of all the synthesized compounds. We confirmed the molecular structure of CzppT through single-crystal X-ray crystallographic analysis. As depicted in Fig. 1, the dihedral angles of the benzene–pyridine and benzene–carbazole bonds (60–80°) revealed that CzppT possessed a rigid core with a highly twisted structure that matched the 3D model of CzppT determined through density functional theory (DFT) optimized using Gaussian 09 at the B3LYP/6-311++G(d,p) level (see below).

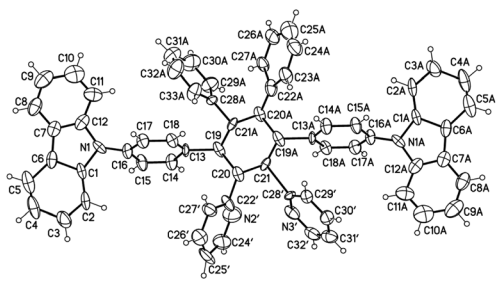

Fig. 1 Molecular structure of CzppT with thermal ellipsoids drawn at the 50% probability level; the dihedral angles of the benzene–pyridine and benzene–carbazole bonds (60–80°) matched the 3D model of CzppT determined through density functional theory (DFT) optimized using Gaussian 09 at the B3LYP/6-311++G(d,p).

Table 1 Crystal data for CzppT based on single-crystal X-ray diffraction (SXRD)

Unit cell dimensions			
a	25.649(9) Å	*α*	90°
b	7.057(3) Å	*β*	105.801(8)°
c	26.695(10) Å	*γ*	90°

Single-crystal XRD analysis

Crystal data for CzppT based on single-crystal X-ray diffraction (SXRD) are arranged as in Table 1: empirical formula, $C_{64}H_{42}N_4$; crystal system, monoclinic; space group, $C1_2/C1$; unit cell dimensions: a = 25.649(9) Å; α = 90°; b = 7.057(3) Å; β = 105.801(8)°; c = 26.695(10) Å; γ = 90°; V = 4649(3) Å^3; Z = 4; 17 658 reflections measured; independent reflections: 4799 [R(int) = 0.0299], which were used in all calculations; density, 1.239 mg m^{-3}; wR^2 = 0.1395 (all data). Intermolecular interactions of CzppT molecules were studied by DFT analysis. There are several intra and intermolecular close contacts in the present molecule, such as C–N=C, C–N, and hydrogen bond with N. The density in 1.239 mg m^{-3} that could be caused by intramolecular interaction of CzppT molecules in different bond lengths. In the structure, an N atom is coordinated in a pyramid by three C atoms of cyclopentane and phenyl groups and one sp^2-C atom. The crystal structure is further stabilized by intra–inter molecular interactions in the solid state. This can also be confirmed using optical absorption and fluorescence properties in solution and solid form in the following discussion.

Theoretical calculations

DFT (Gaussian 09 program package) was used for optimization at the B3LYP/6-311++G(d,p) level of theory, and studying the geometrical and electronic properties of CzppT at the molecular level. As revealed in Fig. 2, the geometry of the dipyridine and carbazole units in the hexaphenylbenzene derivative led to significant twisting of the center core (*i.e.*, a non-planar structure). In addition, the DFT-derived dihedral angles of the carbazole–benzene, pyridine–benzene, and benzene–benzene bonds were 61.4, 64.3, and 69.8°, respectively, quite similar to the experimental (single-crystal XRD analysis) dihedral angles (*ca.* 67.5, 76.0, and 74.3°, respectively), confirming (i) the limited π conjugation between the 4,4″ position of the carbazole unit and the central core and (ii) a twisted structure that prevented intramolecular charge transfer between the carbazole and pyridine units. Thus, we expected CzppT to show a wide HOMO–LUMO energy gap and a high value of T_1. Because of its geometrical constraints, CzppT displayed limited inter- and intra-molecular π conjugation and suppressed molecule recrystallization—features that are anticipated to improve the morphological stability of its thin films in devices. We obtained HOMO and LUMO density maps from 6-311++G(d,p) calculations with the B3LYP functional.

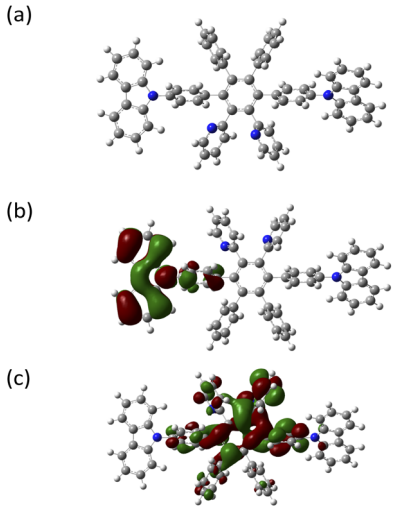

Fig. 2 (a) Optimized geometries of the dipyridine and carbazole units in the hexaphenylbenzene derivative and calculated (b) HOMO and (c) LUMO density maps for CzppT, according to DFT calculations at the B3LYP/6-311++G level. The HOMO and LUMO were distributed on the carbazole unit of the electron-rich fragment and the pyridine unit and central benzene core, respectively.

Fig. 2 displays the HOMO (Fig. 2b) and LUMO (Fig. 2c) of the optimized molecular structure of CzppT; we visualized these molecular orbitals using GaussView. The HOMO was distributed on the carbazole unit of the electron-rich fragment; the LUMO was localized predominantly on the pyridine unit and central benzene core. Thus, electron localization of the HOMO and LUMO of CzppT appeared to involve a pyridine moiety and the carbazole π system, respectively. Therefore, we expected CzppT to exhibit photophysical properties similar to those of its individual pyridine and carbazole components (*i.e.*, as a bipolar material).[28]

Thermal analysis

TGA and DSC were used to investigate the thermal properties of the hexaphenylbenzene derivative. CzppT did not display a glass transition at temperatures up to 350 °C. Notably, the thermal decomposition temperature (T_d, 5% weight loss) of CzppT (480 °C) suggested that the use of this molecule as a host material would enhance the thermal stability of its devices; this thermal stability (Fig. 3) was directly related to the large molecular size after the introduction of the carbazole unit and central core. Because operating temperatures exceeding the thermal stability of the active organic materials will induce device failure, the value of T_d of 480 °C for CzppT suggested that it would be more thermally stable than many other carbazole-based host materials [*e.g.*, the common host material mCP (T_d = 360 °C; Table 2)] when used as a host material in PhOLEDs. The glass transition temperature (T_g) of CzppT can be found at about 260 °C by differential thermal analysis (DSC) measurements, that large than T_g of mCP.

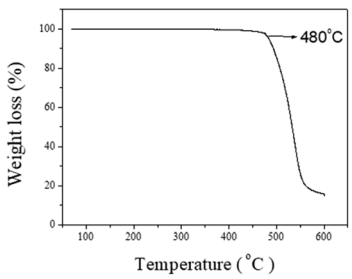

Fig. 3 TGA thermogram of CzppT recorded at a heating rate of 10 °C min^{-1}. CzppT molecules as a host material enhanced thermal stability; this thermal stability was directly related to the introduction of the carbazole unit and central core; the value of T_d was 480 °C for CzppT.

Optical properties

Fig. 4 displays the room-temperature absorption spectrum of CzppT (1×10^{-5} M in THF), its fluorescence spectrum in dilute 2-methyltetrahydrofuran (2-MeTHF; excitation wavelength: 294 nm), and its phosphorescence spectrum in dilute 2-MeTHF (excitation wavelength: 344 nm) at 77 K. In the absorption spectrum, the electronic transitions of CzppT resulted in five absorptions at 244, 294, 303, 344, and 362 nm that are nearly identical to those of the unsubstituted carbazole monomer and, thus, can be attributed to n–π* and π–π* transitions.[29] We attribute the absorption at 244 nm to the benzene π–π* transition; its location in the low wavelength region confirms that the hexaphenylbenzene unit is effective in controlling the extension of the conjugation length. We attribute the absorptions in the range from 294 to 362 nm to the carbazole moiety. Thus, the optical energy gap, or the HOMO–LUMO energy gap, of CzppT was wide, from 6.3 to 3.0 eV; we determined the HOMO and LUMO energies using ultraviolet photoelectron spectroscopy (UPS; Thermo VG-Scientific, Sigma Probe) and the UV-Vis absorption edge using a PerkinElmer Lambda UV-Vis spectrometer, respectively. Upon UV excitation, the maximum emission peaks ranged from 349 to 365 nm in the deep-blue region with respect to the carbazole monomer and benzene units; we observed a red-shifted spectrum. The phosphorescence emission peaks of CzppT in solution (1×10^{-5} M in 2-MeTHF) appeared at 411, 438, and 464 nm; we used the highest-energy phosphorescence emission—the first peak at 411 nm—to calculate the triplet energy level of the highest energy 0–0 phosphorescent emission measured in the 2-MeTHF matrix at 77 K.[30]

The blue-region phosphorescence suggested that the hexaphenylbenzene unit effectively controlled the extension of the π-conjugation. The steric effects of the hexaphenylbenzene unit were minimized through the twisted structure of 4,4″-positions of the carbazole unit with respect to the 2′,3′-positions of the pyridine moiety, thereby giving a triplet energy value of 3.0 eV for CzppT. Because high triplet energy can effectively prevent back energy transfer between host and guest molecules,[26] decreasing the degree of π-conjugation of the host materials should be limited to achieve a triplet energy level higher than that of the triplet emitter. Unlike the situation when mCP is used as a host (T_1 = *ca.* 2.9 eV), CzppT provides a high energy gap and a triplet excited state (3.0 eV) that might avoid T_1–S_1

Table 2 Physical properties of CzppT and the common host material mCP

Compound	T_d (°C)	T_g (°C)	Band gap (eV)	E_T (eV)	HOMO (eV)	LUMO (eV)
CzppT	480	260	3.3	3.0	6.3	3.0
mCP	360	55	3.5	2.9	5.9	2.4

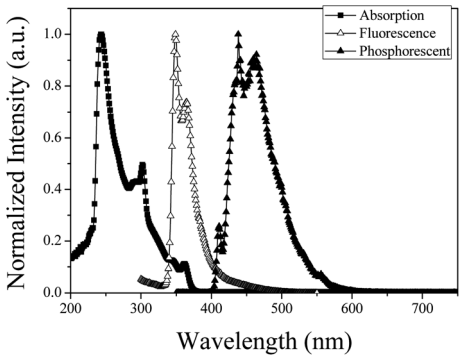

Fig. 4 Normalized spectra of CzppT: UV-Vis absorption in THF solution; fluorescence (ex. = 294 nm) in dilute 2-MeTHF solution; and phosphorescence in dilute 2-MeTHF (ex. = 344 nm) at 77 K.

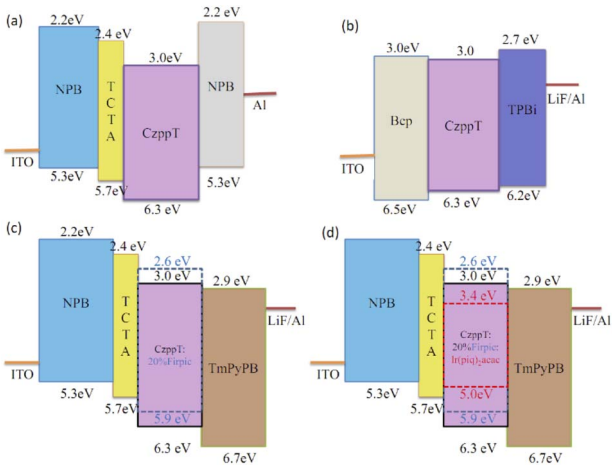

Fig. 5 Design strategy of optimized exciton allocation in relative HOMO/LUMO energy levels of the materials used for the (a) hole-only, (b) electron-only, (c) blue PhOLED, and (d) white PhOLED devices.

reversing and T_1–T_1 annihilation; Table 2 compares the energy levels of these materials. Moreover, the energy level can be tuned by introducing heterocyclic cores; here, we decreased the singlet–triplet exchange energy (S_1–T_1) by introducing two pyridine nitrogen atoms into the central core, consistent with DFT calculations. Accordingly, in this study we used dicarbazole, a well-known electron donor, as a building block to develop a host material possessing attractive carrier transport properties and a high triplet energy level.[31] In addition to the need for a high value of T_1, a good host material must have a favorable exchange energy—one as low as possible—to allow for both charge injection into the host and efficient triplet emission from a dispersed triplet emitter. Because its value of T_1 was higher than that of the commonly used triplet blue-emitter FIrpic (T_1 = *ca.* 2.6 eV), CzppT with a T_1 of 3.0 eV appeared to be a suitable host for use in a device setting.[32]

Hole- and electron-only devices

The current density in a device generally depends on the hole and electron densities. Thus, to verify the charge transfer characteristics of CzppT as a bipolar material, we determined its hole and electron mobilities in terms of its current density–voltage (*I–V*) characteristics. We fabricated hole-only (Fig. 5a) and electron-only (Fig. 5b) devices having the configurations ITO/NPB (30 nm)/TCTA (5 nm)/CzppT (50 nm)/NPB (20 nm)/LiF (0.8 nm)/Al (200 nm) and ITO/Bcp (30 nm)/CzppT (50 nm)/TPBi (20 nm)/LiF (0.8 nm)/Al (200 nm), respectively.[33] In the hole-only device, the low electron affinity (EA) of NPB (2.2 eV) ensured that there would be no electron injection from the Al cathode to the NPB layer; only holes could be injected from the anode, without light emission originating from the organic layers when the holes or electrons passed through the organic layers. In contrast, only electrons were injected into the organic layers in the electron-only devices, because Bcp possesses a large ionization potential (IP) of 6.5 eV. In the electron-only device, Bcp acted as a hole-blocker, inhibiting the injection of holes from the ITO anode to the Bcp layer. Fig. 7 presents the *I–V* curves of the hole- and electron-only devices prepared with CzppT as the charge transport material. The electron current density was high in the CzppT-containing hole- and electron-only devices, indicating that the introduction of the dipyridine groups provided CzppT with good electron injection and transport capabilities, potentially decreasing the electron deficiency of its corresponding OLEDs.

A comparison of the hole and electron current densities revealed that the electron-only device exhibited a significantly lower threshold voltage and a higher current density relative to those of the hole-only device (Fig. 6). Nevertheless, in addition to the hole transport properties, we still observed a positive effect on the hole current density in the hole-only device, resulting mainly from the presence of the carbazole donor units. Such significantly higher electron transport would presumably improve the hole/electron balance in PhOLEDs. Because of electron and hole transport being facilitated in the devices, we confirmed that CzppT was indeed a bipolar material.

Electroluminescence properties

To assess the utility of CzppT as a host and bipolar material for PhOLEDs, blue and white PhOLEDs were fabricated incorporating CzppT as a host material. In these blue and white

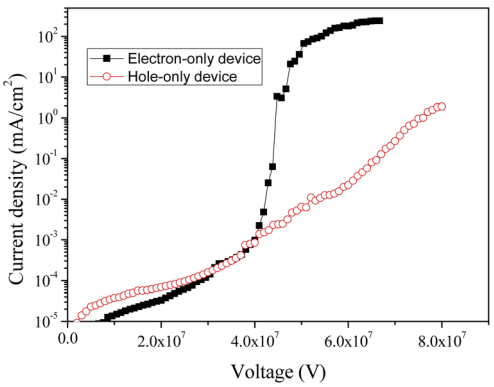

Fig. 6 Current density–voltage (*I*–*V*) characteristics of hole- and electron-only devices. The electron current density was high in the CzppT-containing hole- and electron-only devices. A comparison of the current densities revealed that the electron-only device exhibited higher current density, and that from the properties of hole- and electron-only devices CzppT was indeed a bipolar material.

phosphorescent devices, we doped FIrpic and Ir(piq)$_2$acac, with optimized concentrations of 20 and 0.14%, respectively, as emitters in the host layer. We also employed NPB as the HTL and TCTA as the hole injection layer to enhance the electron injection and transport from the cathode to the emitting layer; we used TmPyPB as the ETL to improve the external quantum efficiency, current efficiency, brightness, and power efficiency. We tested CzppT as the host material in blue (Fig. 5c) and white (Fig. 5d) PhOLEDs having device structures ITO/NPB (45 nm)/TCTA (5 nm)/CzppT:20% FIrpic (30 nm)/TmPyPB (45 nm)/LiF (0.8 nm)/Al (200 nm) and ITO/NPB (45 nm)/TCTA (5 nm)/CzppT:20% FIrpic:0.14% Ir(piq)$_2$acac (30 nm)/TmPyPB (45 nm)/LiF (0.8 nm)/Al (200 nm), respectively. The current efficiency–current density characteristics of the blue device **c** revealed (Fig. 7a) a maximum efficiency of 24.8 cd A^{-1} and a power efficiency of 23 lm W^{-1} at 0.025 mA cm^{-2}; Fig. 7b presents the

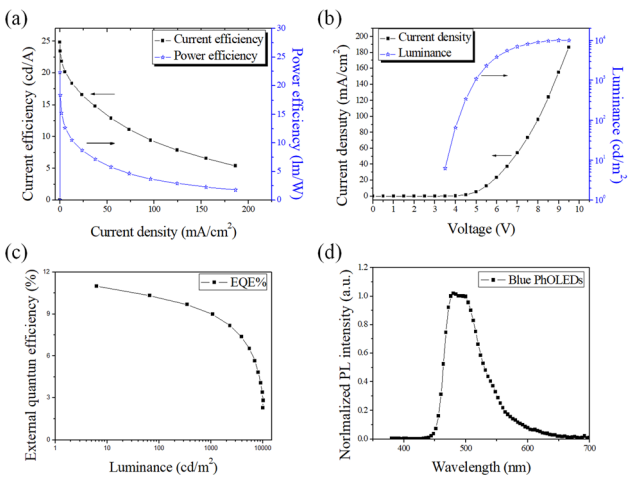

Fig. 7 (a) Efficiency–current density and (b) current density and brightness plotted with respect to applied voltage, (c) external quantum efficiency, and (d) EL spectral characteristics of CzppT when used as a host in blue phosphorescent devices.

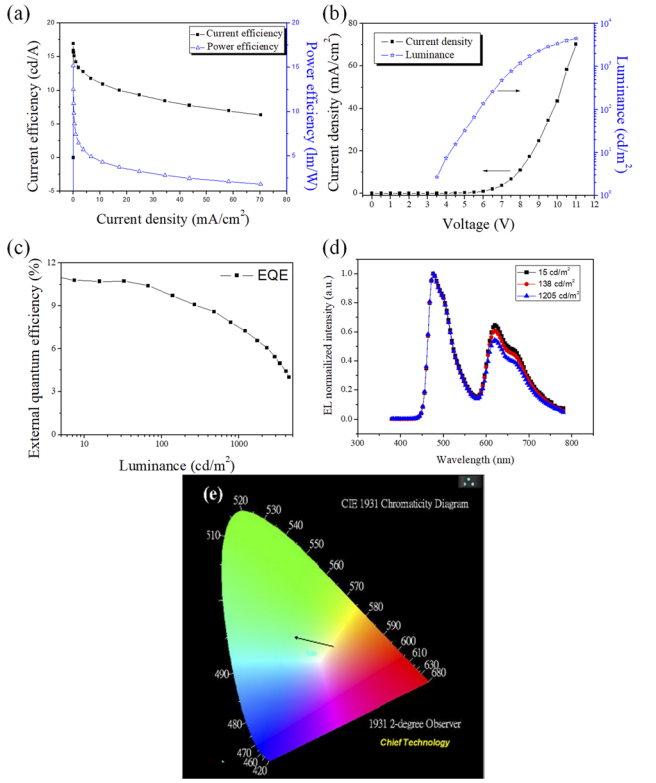

Fig. 8 (a) Efficiency–current density and (b) current density and brightness plotted with respect to applied voltage, (c) external quantum efficiency, and (d) EL spectral characteristics of CzppT when used as a host in white phosphorescent devices and (e) CIE changes with increasing the work voltage.

corresponding current density–voltage and luminance–voltage characteristics. The maximum external quantum efficiency of the blue emitting device was 11.0% (Fig. 7c); its emission was close to sky-blue, with respect to the peak wavelengths of 476 and 500 nm from the FIrpic complex (Fig. 7d), with CIE coordinates (*x*, *y*) of (0.18, 0.41). The current efficiency–current density characteristics of the representative white device **d** (Fig. 8a) revealed a maximum efficiency of 16.8 cd A^{-1} and a power efficiency of 15.1 lm W^{-1} at 0.015 mA cm^{-2}; Fig. 8b presents the associated current density–voltage and luminance–voltage characteristics. The external quantum efficiency, and EL spectral characteristics of CzppT are shown in Fig. 8c and d, respectively.

In Fig. 8d and e, the EL and CIE change with increasing the work voltage. The maximum external quantum efficiency of the white-emitting device was 11.3%, with the emission wavelength contributed by the FIrpic and Ir(piq)$_2$acac units, with CIE coordinates (*x*, *y*) ranging from (0.32, 0.36) to (0.31, 0.37) at voltages from 3.5 to 11 V. Here, the white electroluminescence occurred *via* direct charge recombination with triplet exciton formation in the blue FIrpic complex combined with partial energy transfer from FIrpic to the red emitting dopant Ir(piq)$_2$acac at a low concentration. The data imply a way to direct the formation of triplet excitons in the emitting layer—through the high triplet energy level of CzppT—to prevent the

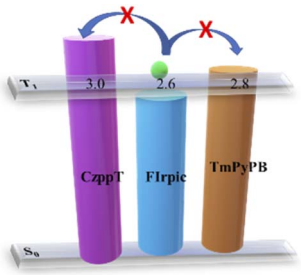

Fig. 9 Triplet energy levels of CzppT, FIrpic, and TmPyPB; whole strong charge capture by red dyes leads to the excessive energy transfer from FIrpic emitters through CzppT, reducing the reverse intersystem crossing through triplet energy. S_0 and T_1 refer to ground and the first triplet states, respectively.

process of reverse intersystem crossing from the triplet excited state (T_1) to the singlet excited state (S_1) and triplet–triplet (T_1–T_1) annihilation to generate a singlet exciton, thereby leading to increased device efficiency and electroluminescence, as revealed in Fig. 9. Presumably, devices **c** and **d** incorporating TmPyPB with high triplet level (2.8 eV) as the ETL provided strong control over the exciton from FIrpic or $Ir(piq)_2acac$ to the ETL, and improved EL efficiencies.

Conclusions

This contribution reports the synthesis and characterization of a new hexaphenylbenzene end-capped with a dicarbazole derivative, named CzppT, and, consequently, fabrication of a high-performance device. The dicarbazole derivative has small singlet–triplet exchange energies (ΔE_{ST}) within pyridine moieties which promote electron injection into and electron transport within pyridine-containing ETLs to possess high triplet energy levels (3.0 eV) and thermal stability with a value of T_d of 480 °C. We successfully fabricated a blue PhOLED device having the configuration ITO/NPB (45 nm)/TCTA (5 nm)/CzppT:20% FIrpic (30 nm)/TmPyPB (45 nm)/LiF (0.8 nm)/Al (200 nm); it exhibited a maximum efficiency of 24.8 cd A^{-1}, a power efficiency of 23 lm W^{-1} at 0.025 mA cm^{-2}, and a maximum external quantum efficiency of 11.0% with CIE coordinates (x, y) of (0.18, 0.41). In addition, we also prepared a white PhOLED device having the configuration ITO/NPB (45 nm)/TCTA (5 nm)/CzppT:20% FIrpic:0.14% $Ir(piq)_2acac$ (30 nm)/TmPyPB (45 nm)/LiF (0.8 nm)/Al (200 nm); it exhibited a maximum efficiency of 16.8 cd A^{-1}, power efficiency of 15.1 lm W^{-1} at 0.015 mA cm^{-2}, maximum external quantum efficiency of 11.3%, and CIE coordinates (x, y) ranging from (0.32, 0.36) to (0.31, 0.37) at voltages from 3.5 to 11 V. These results indicate that CzppT can be a bipolar and simple devices structure to manufacture high-performance OLEDs in the future.

Author contributions

Conceptualization, methodology, investigation and writing—original draft preparation, Hsin-Yi Wen; formal analysis, writing—review and editing, Hsin-Yi Wen and Shou-Yi Ho.

Conflicts of interest

There are no conflicts to declare.

Acknowledgements

This study was financially supported by a grant from the Ministry of Science and Technology of Taiwan and by the grant MOST-111-2221-E-992-086- and MOST 110-2222-E-309-001-.

References

1 S. Kagatikar and D. Sunil, *J. Mater. Sci.*, 2022, **57**, 105–139.
2 R. Su, S. H. Park, X. Ouyang, S. I. Ahn and M. C. McAlpine, *Sci. Adv.*, 2022, **8**, eabl8798.
3 U. Giovanella, M. Pasini and C. Botta, in *Applied Photochemistry*, Springer, 2016, pp. 145–196.
4 Z. Ye, Z. Ling, M. Chen, J. Yang, S. Wang, Y. Zheng, B. Wei, C. Li, G. Chen and Y. Shi, *RSC Adv.*, 2019, **9**, 6881–6889.
5 K. M. Kuznetsov, M. I. Kozlov, A. N. Aslandukov, A. A. Vashchenko, A. V. Medved'ko, E. V. Latipov, A. S. Goloveshkin, D. M. Tsymbarenko and V. V. Utochnikova, *Dalton Trans.*, 2021, **50**, 9685–9689.
6 X. Zhang, J. An, Y. Xu, Y. Wang, Y. Lu, Y. Qin, W.-Y. Lai, Y. Chen and W. Huang, *J. Mater. Chem. C*, 2021, **9**, 2190–2197.
7 J. Bauri, R. B. Choudhary and G. Mandal, *J. Mater. Sci.*, 2021, **56**, 18837–18866.
8 S. C. Xia, R. C. Kwong, V. I. Adamovich, M. S. Weaver and J. J. Brown, OLED device operational lifetime: Insights and challenges, In *2007 IEEE International Reliability Physics Symposium Proceedings. 45th Annual*, IEEE, 2007, pp. 253–257.
9 S. Sudheendran Swayamprabha, D. K. Dubey, R. A. K. Yadav, M. R. Nagar, A. Sharma, F. C. Tung and J. H. Jou, *Adv. Sci.*, 2021, **8**, 2002254.
10 H. Uoyama, K. Goushi, K. Shizu, H. Nomura and C. Adachi, *Nature*, 2012, **492**, 234–238.
11 K. Goushi, K. Yoshida, K. Sato and C. Adachi, *Nat. Photonics*, 2012, **6**, 253–258.
12 C.-H. Chen, B.-Y. Lin, N. T. Tierce, M.-k. Leung, T.-L. Chiu, C. J. Bardeen and J.-H. Lee, *Chem. Eng. J.*, 2022, **427**, 130889.
13 J.-W. Kang, S.-H. Lee, H.-D. Park, W.-I. Jeong, K.-M. Yoo, Y.-S. Park and J.-J. Kim, *Appl. Phys. Lett.*, 2007, **90**, 223508.
14 W. Jiang, L. Duan, J. Qiao, G. Dong, D. Zhang, L. Wang and Y. Qiu, *J. Mater. Chem.*, 2011, **21**, 4918–4926.
15 Y. Tao, Q. Wang, Y. Shang, C. Yang, L. Ao, J. Qin, D. Ma and Z. Shuai, *Chem. Commun.*, 2009, 77–79.
16 H.-F. Chen, S.-J. Yang, Z.-H. Tsai, W.-Y. Hung, T.-C. Wang and K.-T. Wong, *J. Mater. Chem.*, 2009, **19**, 8112–8118.
17 S. Watanabe and J. Kido, *Chem. Lett.*, 2007, **36**, 590–591.
18 K. J. Thomas, M. Velusamy, J. T. Lin, C. Chuen and Y.-T. Tao, *J. Mater. Chem.*, 2005, **15**, 4453–4459.
19 J. K. Park, K. H. Lee, S. Kang, J. Y. Lee, J. S. Park, J. H. Seo, Y. K. Kim and S. S. Yoon, *Org. Electron.*, 2010, **11**, 905–915.
20 M.-X. Yu, J.-P. Duan, C.-H. Lin, C.-H. Cheng and Y.-T. Tao, *Chem. Mater.*, 2002, **14**, 3958–3963.

21 S.-P. Huang, T.-H. Jen, Y.-C. Chen, A.-E. Hsiao, S.-H. Yin, H.-Y. Chen and S.-A. Chen, *J. Am. Chem. Soc.*, 2008, **130**, 4699–4707.
22 H. Sasabe and J. Kido, *Chem. Mater.*, 2011, **23**, 621–630.
23 T. Yamamoto, T. Maruyama, Z.-H. Zhou, T. Ito, T. Fukuda, Y. Yoneda, F. Begum, T. Ikeda and S. Sasaki, *J. Am. Chem. Soc.*, 1994, **116**, 4832–4845.
24 H. Xu, P. O. Lartey, Y. Wu, X. Liang, F. Zhang, D. Li, B. Li, Z. Zhang, S. Wang, K. Guo and J. Ma, *Dyes Pigm.*, 2021, **193**, 109483.
25 K. J. Thomas, J. T. Lin, Y. T. Tao and C. W. Ko, *Adv. Mater.*, 2000, **12**, 1949–1951.
26 G. M. Farinola and R. Ragni, *Chem. Soc. Rev.*, 2011, **40**, 3467–3482.
27 J. F. Wolfe and F. Arnold, *Macromolecules*, 1981, **14**, 909–915.
28 W.-Y. Hung, L.-C. Chi, W.-J. Chen, E. Mondal, S.-H. Chou, K.-T. Wong and Y. Chi, *J. Mater. Chem.*, 2011, **21**, 19249–19256.
29 J. Y. Shen, X. L. Yang, T. H. Huang, J. T. Lin, T. H. Ke, L. Y. Chen, C. C. Wu and M. C. Yeh, *Adv. Funct. Mater.*, 2007, **17**, 983–995.
30 W. Jiang, L. Duan, J. Qiao, D. Zhang, G. Dong, L. Wang and Y. Qiu, *J. Mater. Chem.*, 2010, **20**, 6131–6137.
31 S.-J. Su, C. Cai and J. Kido, *Chem. Mater.*, 2011, **23**, 274–284.
32 S. Tokito, T. Iijima, Y. Suzuri, H. Kita, T. Tsuzuki and F. Sato, *Appl. Phys. Lett.*, 2003, **83**, 569–571.
33 M.-S. Lin, L.-C. Chi, H.-W. Chang, Y.-H. Huang, K.-C. Tien, C.-C. Chen, C.-H. Chang, C.-C. Wu, A. Chaskar and S.-H. Chou, *J. Mater. Chem.*, 2012, **22**, 870–876.